Instantaneous quadrature low-coherence interferometry with 3 × 3 fiber-optic couplers

Michael A. Choma, Changhuei Yang, and Joseph A. Izatt

Department of Biomedical Engineering, Duke University, Durham, North Carolina 27708

Received May 30, 2003

We describe fiber-based quadrature low-coherence interferometers that exploit the inherent phase shifts of 3×3 and higher-order fiber-optic couplers. We present a framework based on conservation of energy to account for the interferometric shifts in 3×3 interferometers, and we demonstrate that the resulting interferometers provide the entire complex interferometric signal instantaneously in homodyne and heterodyne systems. In heterodyne detection we demonstrate the capability for extraction of the magnitude and sign of Doppler shifts from the complex data. In homodyne detection we show the detection of subwavelength sample motion. $N \times N$ ($N > 2$) low-coherence interferometer topologies will be useful in Doppler optical coherence tomography (OCT), optical coherence microscopy, Fourier-domain OCT, optical frequency domain reflectometry, and phase-referenced interferometry.

OCIS codes: 110.4500, 120.3180.

Interferometry with broadband light sources has become a widely used technique for imaging of biologic samples by use of time-domain optical coherence tomography[1] (OCT), optical coherence microscopy,[2] Fourier-domain OCT,[3] optical frequency domain reflectometry,[4] color Doppler OCT,[5] and phase-referenced interferometry.[6] In many of these applications, it is useful or necessary to have access to the entire complex interferometric signal to extract amplitude and phase information encoding scatterer locations and (or) motions. Unfortunately, the square-law detector output obtained in conventional OCT systems yields only the real part of the complex signal (in the case of single receiver systems), or the real part and its inverse (in the case of differential receiver systems[7]).

Several methods are available that allow for instantaneous or sequential retrieval of both quadrature components of the complex interferometric signal. These include (1) polarization quadrature encoding,[8] where orthogonal polarization states encode the real and imaginary components; (2) phase stepping,[3] where the reference reflector is serially displaced, thus time encoding the real and imaginary components; and (3) synchronous detection, where the photodetector output is mixed with an electronic local oscillator at the heterodyne frequency. Synchronous detection methods include lock-in detection[5] and phase-locked loops. Polarization quadrature encoding and phase stepping can be generically called quadrature interferometry since the complex signal is optically generated. As such, they are useful in both homodyne and heterodyne systems.

Each of these techniques suffers from shortcomings. Polarization quadrature encoding is instantaneous, but it requires a complicated setup, and it suffers from polarization fading. Phase shifting requires a stable and carefully calibrated reference-arm setup, is not instantaneous, and is sensitive to interferometer drift between phase-shifted acquisitions. Synchronous detection is not instantaneous and depends on the presence of an electronic carrier frequency. Systems based on synchronous detection are thus not useful in an important class of homodyne systems such as *en-face* imaging schemes and those that take advantage of array detection.

In this Letter we present a fiber-based quadrature broadband interferometer that exploits the inherent phase shifts of 3×3 fiber-optic couplers. We present a simple argument to explain interferometric phase shifts in 2×2 and 3×3 Michelson interferometers, and we demonstrate that the outputs of a 3×3 interferometer provide instantaneous access to the entire complex interferometric signal in homodyne and heterodyne systems.

Fused-fiber couplers rely on evanescent-wave coupling to split an input electric field between output fiber paths, according to coupled-mode theory.[9,10] Here we describe a simpler formalism based on conservation of energy that predicts phase shifts for interferometers based on 2×2 and 3×3 couplers. While higher-order couplers (e.g., 4×4) can be used in a manner similar to that described below for 3×3s to acquire the complex interferometric signal, the phase shifts in these couplers can be explained only by coupled-mode theory.

Consider the 2×2 and 3×3 Michelson interferometers illustrated in Fig. 1. The coefficient α_{ab} describes the power transfer from fiber a to fiber b. For example, a 2×2 50/50 coupler has $\alpha_{11} = \alpha_{12} = 1/2$, and a 3×3 33/33/33 coupler has $\alpha_{11} = \alpha_{12} = \alpha_{13} = 1/3$. Ignoring the return loss from the source 50/50 coupler, the optical intensity incident on the nth detector that is due to a single reflection in the sample is

$$I_n = \gamma I_0[\alpha_{11}\alpha_{1n} + \alpha_{12}\alpha_{2n} + 2E(\Delta x)(\alpha_{11}\alpha_{1n}\alpha_{12}\alpha_{2n})^{1/2} \times \cos(2k\Delta x + \phi_n)]. \quad (1)$$

Here k is the optical wave number, Δx is the path-length difference between reflectors in the reference and sample arms, $E(\Delta x)$ is the interferometric envelope (i.e., the magnitude of the complex signal), and ϕ_n is the phase shift between the optically heterodyned fields when $\Delta x = 0$. γ ensures that the total power incident on the reference and sample arms is I_0 and is 1 for a 2×2 and $\gamma = 1/(\alpha_{11} + \alpha_{12})$ for a 3×3. Since the noninterferometric portions of

0146-9592/03/222162-03$15.00/0

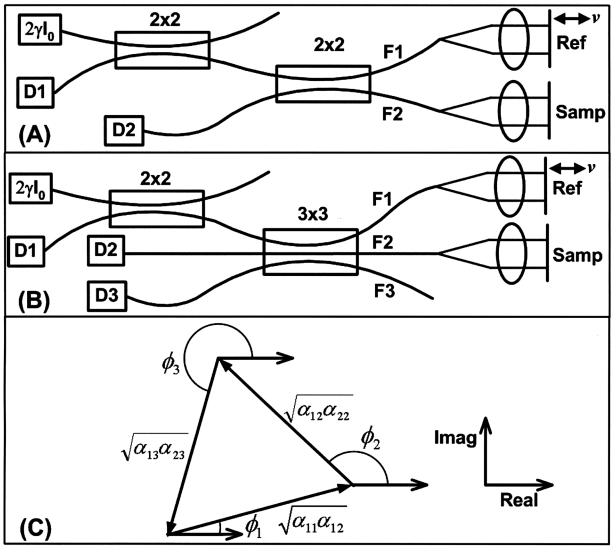

Fig. 1. (A) Conventional differential low-coherence Michelson interferometer based on 2×2 fiber couplers. I_0 is the total power incident on the reference and sample arms. $\gamma = 1$. D, detector; F, fiber. (B) Michelson interferometer based on a 3×3 fiber coupler. $\gamma = 1/(\alpha_{11} + \alpha_{12})$. A circulator may be used in place of the input couplers in both (A) and (B) for increased efficiency.[7] (C) Graphic representation of Eq. (2) for the coupling ratios and intrinsic phase shifts in a 3×3 interferometer.

I_n sum to I_0, the interferometric portions must sum to zero, independently of Δx. Assuming (1) perfect reciprocity (i.e., $\alpha_{ab} = \alpha_{ba}$) and (2) lossless coupling ($\sum_n \alpha_{an} = 1$) in the fiber coupler,

$$\mathrm{Re}\left[\sum_n \sqrt{\alpha_{1n}\alpha_{2n}}\exp(j2k\Delta x)\exp(j\phi_n)\right] = 0\,, \quad (2a)$$

$$\sum_n \sqrt{\alpha_{1n}\alpha_{2n}}\cos(\phi_n) = \sum_n \sqrt{\alpha_{1n}\alpha_{2n}}\sin(\phi_n) = 0\,. \quad (2b)$$

Because variations in $k\Delta x$ rotate the $(\alpha_{1n}\alpha_{2n})^{1/2} \times \exp(j\phi_n)$ vector in the complex plane, Eq. (2a) is true if and only if $(\alpha_{1n}\alpha_{2n})^{1/2}\exp(j\phi_n)$ sums to zero [Eq. (2b)]. Equations (2) demand that $|\phi_1 - \phi_2| = 180°$ for 2×2 couplers regardless of the coupler splitting ratio, while $\phi_m - \phi_n$ is an explicit function of α_{ab} for 3×3 couplers. Equation (2b) can be represented graphically as the sum of three complex vectors with magnitude $(\alpha_{1n}\alpha_{2n})^{1/2}$ and phase ϕ_n [Fig. 1(C)]. Given a set of measured values of α_{ab}, the interferometric phase shifts between coupler arms $\phi_m - \phi_n$ are uniquely determined, since the three vectors correspond to the sides of a triangle whose inner angles are related to $\phi_m - \phi_n$. For example, if $\alpha_{ab} = 1/3$ for all a and b, then the interferometric phase shift between any two output ports of a 3×3 Michelson interferometer is 120°.

Because the phase shifts among I_n are not constrained to be 0° or 180° for interferometers based on 3×3 couplers, the complex interferometric signal can be obtained instantaneously from simultaneous measurements of two or more detector outputs. It should be noted that this can be accomplished with all higher-order $N \times N$ interferometers ($N > 2$) of various topologies (e.g., Michelson, Mach–Zehnder). A straightforward algorithm for reconstructing the complex interferometric signal uses the signal from any two photodetectors. Defining i_n as the interferometric portion of I_n, and assigning any i_n as the real part of the complex signal (denoted i_{Re} below), we may then obtain the imaginary part, $i_{Im} = 2E(\Delta x)(\alpha_{11}\alpha_{1n}\alpha_{12}\alpha_{2n})^{1/2}\sin(2k\Delta x + \phi_n)$, by use of the cosine sum rule as

$$i_{Im} = \frac{i_n \cos(\phi_m - \phi_n) - \beta i_m}{\sin(\phi_m - \phi_n)}\,,$$

$$\beta = \left(\frac{\alpha_{11}\alpha_{1n}\alpha_{12}\alpha_{2n}}{\alpha_{11}\alpha_{1m}\alpha_{12}\alpha_{2m}}\right)^{1/2}. \quad (3)$$

We constructed the setup illustrated in Fig. 1(B) from a superluminescent diode source (OptoSpeed; $\lambda_0 = 1274$ nm, $\Delta\lambda = 28$ nm) and an AC Photonics 3×3 truly fused-fiber coupler. To demonstrate instantaneous quadrature signal acquisition in a heterodyne experiment, we scanned the reference arm at $v = 8.3$ mm/s. The interferometric portions of all three acquired photodetector outputs are illustrated in Fig. 2. When experimentally measured values of α_{ab} were used to solve for the theoretical interferometric phase shifts, these theoretical shifts deviated from the experimental shifts by $\leq 2.5\%$. We noted that $\phi_m - \phi_n$ drifted over the course of minutes to hours, and we hypothesize that these drifts are due to temperature sensitivity of the coupler splitting ratio.

If i_1, i_2, and i_3 are parametrically plotted against one another, a three-dimensional Lissajous curve is formed [Fig. 3(A)]. Time is encoded by the color of the curve: In this experiment the data were captured as Δx increased with time, and thus as time progresses, the curve spirals outward and transitions from green to black to red [Fig. 3(D)]. The curve fills an ellipse [Fig. 3(B)]. The real (i_2) and imaginary parts [calculated from Eqs. (3)] of the interferogram are plotted as a Lissajous curve in Fig. 3(C) and were used to calculate the magnitude and phase as plotted in Fig. 4. The time derivative of the phase yields the Doppler shift $f_d = 2v/\lambda$ generated by the scanning reference mirror. The experimentally calculated Doppler shift (Fig. 4) agrees well with the predicted value, based on the calibrated scan velocity of the reference arm.

We also demonstrated 3×3 instantaneous quadrature signal acquisition in a homodyne experiment by positioning a nonscanning reference mirror ($v = 0$) such that Δx corresponded to the middle of an interferogram.

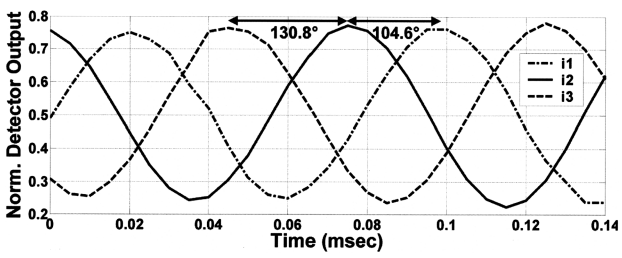

Fig. 2. Interferometric detector outputs of a 3×3 Michelson interferometer in a heterodyne experiment.

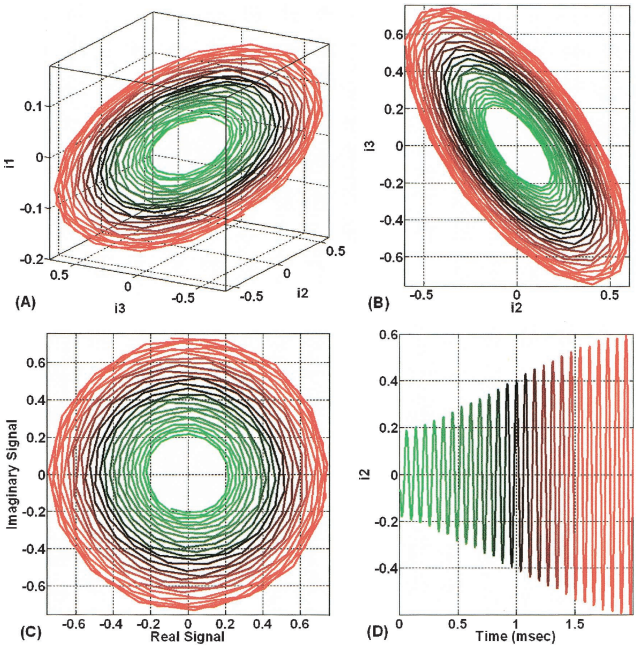

Fig. 3. (A) Three-dimensional Lissajous plots of the interferometric signal from three photodetectors in a 3×3 Michelson interferometer. Time is color coded (green–black–red). (B) Lissajous plot of i_3 versus i_2. (C) Real and imaginary signals calculated from i_2 and i_3. (D) i_2 versus time plotted with color coding.

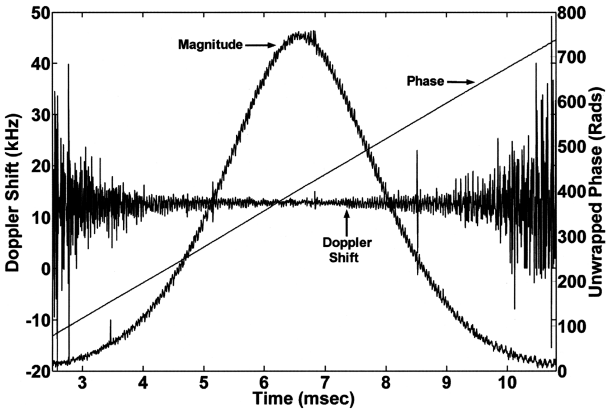

Fig. 4. Magnitude, phase, and Doppler shift of complex heterodyne interferometric signal calculated from outputs of the 3×3 interferometer. The Doppler shift is calculated from the numerical derivative of the phase and is in good agreement with the predicted value of 13 kHz.

We then recorded the outputs i_2 and i_3 for 10 s and used Eqs. (3) to reconstruct amplitude and phase. Because of interferometer arm-length drifts of the order of $\sim\lambda$, the phase of the complex interferometric signal varied by $\sim 2\pi$, whereas the magnitude remained steady (mean 1.52, variance 1.96×10^{-4}; see Fig. 5). This result demonstrates the potential utility of $N \times N$ interferometers in homodyne OCT approaches such as optical coherence microscopy, Fourier-domain OCT, and optical frequency-domain interferometry.

Although higher-order $N \times N$ interferometers are less efficient with source light than conventional 2×2 interferometers, they are more efficient at collecting light reflected from the sample and may thus be advantageous in sample exposure-limited applications such as retinal imaging. For example, the 3×3 interferometer in Fig. 1(b) delivers only $1/6$ of the source light to the sample but collects $1/3 + 1/3 + 1/3\,1/2 = 83\%$ of the light returning from the sample. The same interferometer without the input 2×2 coupler is an attractive alternative that delivers 33% of the source light to the sample, collects 66% of the reflected light, and still performs instantaneous quadrature detection with two detector signals (D_2 and D_3) as inputs to Eq. (3).

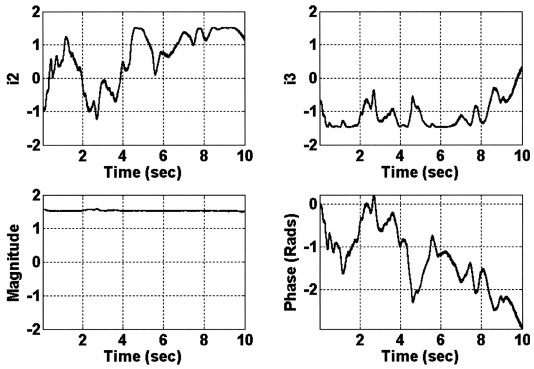

Fig. 5. Magnitude and phase of the complex interferometric signal in a homodyne experiment. The reference arm was not scanned; small random motions of the reference and sample mirrors led to variations in the interferometric phase. Application of the algorithm of Eqs. (3) allowed for clean extraction of magnitude and phase from outputs D_2 and D_3 of a 3×3 interferometer. The magnitude was constant (mean 1.52, variance 1.96×10^{-4}), whereas small mirror motions led to $\sim\pi$ in phase.

In conclusion, $N \times N$ interferometers allow for instantaneous optical extraction of magnitude and phase information in a compact and simple design. Their advantages are particularly compelling in Fourier-domain OCT and optical frequency domain reflectometry, where they will allow for optical resolution of complex-conjugate ambiguity without phase stepping.

This work was supported by National Institutes of Health grant R24-EB000243. J. A. Izatt's e-mail address is jizatt@duke.edu.

References

1. D. Huang, E. A. Swanson, C. P. Lin, J. S. Schuman, W. G. Stinson, W. Chang, M. R. Hee, T. Flotte, K. Gregory, and C. A. Puliafito, Science **254,** 1178 (1991).
2. J. A. Izatt, M. D. Kulkarni, H. W. Wang, K. Kobayashi, and M. V. Sivak, IEEE J. Sel. Top. Quantum Electron. **2,** 1017 (1996).
3. M. Wojtkowski, A. Kowalczyk, R. Leitgeb, and A. F. Fercher, Opt. Lett. **27,** 1415 (2002).
4. S. R. Chinn, E. A. Swanson, and J. G. Fujimoto, Opt. Lett. **22,** 340 (1997).
5. J. A. Izatt, M. D. Kulkami, S. Yazdanfar, J. K. Barton, and A. J. Welch, Opt. Lett. **22,** 1439 (1997).
6. C. Yang, A. Wax, M. S. Hahn, K. Badizadegan, R. R. Dasari, and M. S. Feld, Opt. Lett. **26,** 1271 (2001).
7. A. M. Rollins and J. A. Izatt, Opt. Lett. **24,** 1484 (1999).
8. Y. H. Zhao, Z. P. Chen, Z. H. Ding, H. W. Ren, and J. S. Nelson, Opt. Lett. **27,** 98 (2002).
9. A. W. Snyder, J. Opt. Soc. Am. **62,** 1267 (1972).
10. S. K. Sheem, J. Appl. Phys. **52,** 3865 (1981).